Attitude Control for a Micromechanical Flying Insect via Sensor Output Feedback

L. Schenato W.C. Wu S.S. Sastry

Department of EECS, University of California, Berkeley, CA 94720
{*lusche, wcwu, sastry*}*@eecs.berkeley.edu*

Abstract

Body rotation and orientation sensing mechanisms used by flying insects are introduced and their mathematical models are presented. The analysis and simulations of these models showed the feasibility of using such biologically inspired approaches to build biomimetic gyroscopes and angular position detectors. Further, an approximate rigid body model for the insect body dynamics is developed so that attitude stabilization techniques for a flying robotic insect can be tested to illustrate the utility of these novel sensor architectures. To the authors' knowledge, this is the first attempt in using output feedback from biomimetic devices such as ocelli and halteres to achieve attitude stabilization.

1 Introduction

Micro aerial vehicles (MAVs) have drawn a great deal of attention in the past decade due to the quick advances in microtechnology and several groups have worked on MAVs based on fixed and rotary wings [4]. However, flapping flight provides superior maneuverability that would be beneficial in obstacle avoidance and for navigation in small spaces. Therefore, the UC Berkeley Micromechanical Flying Insect (MFI) project uses biomimetic principles to develop a flapping wing MAV that will be capable of sustained autonomous flight [1],[12]. One important concern in designing the components of the MFI is their power consumption. Current power budget for the MFI is $20mW$ and the majority of this power will be allocated to the actuation of the two wings.

On the other hand, the sensory system of the MFI, which is crucial for stabilizing flight, should consume little power. The power requirements of off-the-shelf micro sensors are generally too expensive for the MFI. At present, piezo-actuated biomimetic angular rate sensors for use on the MFI have been constructed [11]. Another biomimetic device called ocelli, which is currently being implemented, consists of four photoreceptors to sense the light intensity in the surrounding to estimate the orientation of the MFI. Both sensors have the virtues of simple design, easy implementation, low power consumption, and high performance. This paper first presents the modeling of these two types of biologically inspired sensors and then proposes a close-loop attitude control scheme using the sensor output as feedback.

2 Insect Flight Dynamics

Flight dynamics of flapping insects is still an open area of research [7] due to the difficulties of measuring aerodynamic forces on real flying insects, and of validating proposed theoretical models. In this work we model the dynamics of a flying insect as a rigid body subject to external forces. Albeit wings do move relative to the insect body, their mass is within $1-5\%$ of total insect mass and hence their effect on the insect dynamics is relatively small and can be neglected. Therefore, we assume that the insect body motion evolves according to the rigid body motion equations subject to external forces relative to its center of mass [5]. The external forces acting on an insect are the aerodynamic forces generated by the wings, the gravity force, and the body viscous drag. Since we are interested in attitude control, gravity does not play a role. Also, we deal mainly with slow body rotations in this work, angular viscous forces are neglected. The aerodynamic forces generated by flapping wings are highly time-varying within a single wingbeat and they can not be controlled instantaneously. However, preliminary work on wing kinematics seems to indicate that it is possible to control the *mean* value of these forces, in particular torques, over a full wingbeat [8]. Therefore, in this work we assume that we have full control of the aerodynamic torques. Moreover, since the motion of the insect is slow relative to the motion of the wings, we assume that these torques can be controlled continuously. Summing up, the dynamics of the attitude of a flapping insect is modeled as follows:

$$\begin{array}{rcl} \dot{R} & = & R\hat{\omega}^b \\ \dot{\omega}^b & = & I_b^{-1}(\tau^b - \omega^b \times I_b\omega^b) \\ \tau^b & = & u \\ \hat{\omega}^b & = & \begin{bmatrix} 0 & \omega_z^b & -\omega_y^b \\ -\omega_z^b & 0 & \omega_x^b \\ \omega_y^b & -\omega_x & 0 \end{bmatrix} \end{array} \quad (1)$$

where $\omega^b = [\omega_x^b\, \omega_y^b\, \omega_z^b]^T$ is the angular velocity of the insect body relative to the body frame B, $\tau^b \in R^3$ is the total external torque relative to the body frame B attached to the center of mass of the insect body, $I_b \in R^{3\times 3}$ is the moment of inertia of the insect body relative to the body frame B, ω^b is the insect body angular velocity relative to the body frame B, $u \in R^3$ is the control input vector, and $R \in SO(3) = \{R \in R^{3\times 3} : R^TR = I, \det R = +1\}$ is the rotation matrix representing the orientation of the insect body frame B relative to the fixed frame A. In particular, let $v^b = [x_b\, y_b\, z_b]^T$ and $v^a = [x_a\, y_a\, z_a]^T$ the coordinates of a vector $v \in R^3$ relative to the body frame B and the fixed frame A, respectively. Then, these coordinates satisfy the following transformations:

$$\begin{array}{rcl} v_a & = & Rv_b \\ v_b & = & R^Tv_a \end{array} \quad (2)$$

As shown in Figure 1, the coordinates of the z-axis $v_z^b = [0\,0\,1]^T$ attached to the body frame relative to

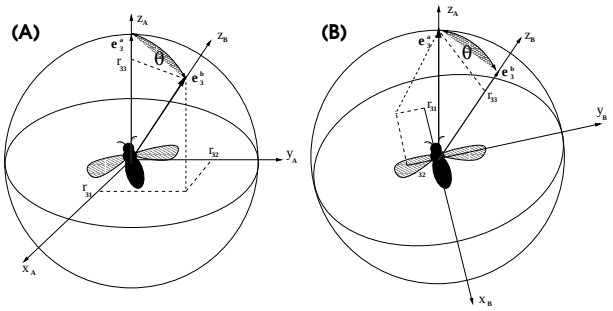

Figure 1: Fixed frame and body frame coordinates representation

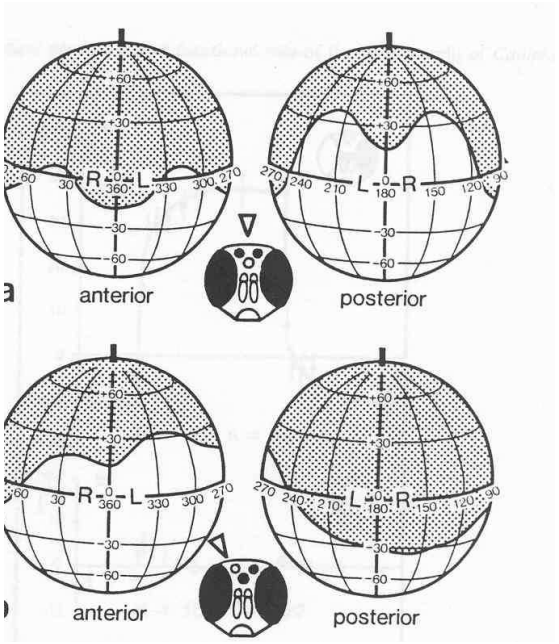

Figure 2: Head of a blowfly and the field of reception of its ocelli (curtesy from [10])

the fixed frame A are $v_z^a = Rv_z^b = [r_{13}\, r_{23}\, r_{33}]^T$, while the coordinates of the z-axis $w_z^a = [0\,0\,1]^T$ attached to the fixed frame relative to the body frame B are $w_z^b = R^T w_z^a = [r_{31}\, r_{32}\, r_{33}]^T$. Note that $w_z^b \neq v_z^a$.

3 Ocelli

3.1 Morphology

The ocelli are sensory organs present in many flying insects. This system consists of three wide angle photoreceptors placed on the head of the insect (see Figure 3.1). They are oriented in such a way that they collect light from different regions of the sky (see Figure 3.1). Albeit the exact physiology of the ocelli and their scope in insect flight is still not completely unveiled, it is believed that they play a fundamental role in attitude stabilization, in particular horizon stabilization in some insects [10].

Biologists believe that ocelli estimate the orientation of the insect with respect to the sky by comparing the intensity of light measured by the different photoreceptors. Their argument is based on the assumption that, as a first approximation, the intensity

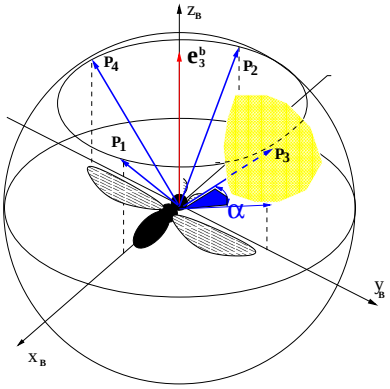

Figure 3: Graphical rendering of ocelli present in flying insects. Four photoreceptors, represented as $P1, P2, P3, P4$, collect light from different regions of the sky. The shadowed area indicates such a region for photoreceptor $P3$.

of light measured by the photoreceptors, I, is only a function of its latitude θ relative to the light source (*i.e.* the sun).

3.2 Modeling

Any point P in the sky can be represented in polar coordinates (r, θ, ψ) where $r \in R^+$ is the radius of the celestial sphere, $\theta \in [0, \pi]$ is the latitude, and $\psi \in [0, 2\pi]$ is the longitude, relative to the fixed frame A. Without loss of generality, the radius of the celestial sphere is normalized to unity, *i.e.* $r = 1$. Alternatively, the same point can be written in Cartesian coordinates $p = (x_P, y_P, z_P), ||p|| = 1$. The transformation from polar to Cartesian coordinates is given by:

$$\begin{array}{rcl} x_P & = & \sin\theta\cos\psi \\ y_P & = & \sin\theta\sin\psi \\ z_P & = & \cos\theta \end{array} \tag{3}$$

The ocelli sensory system is modeled as four ideal photoreceptors, called P_1, P_2, P_3, P_4, fixed with respect to the body frame B, each measuring the light intensity from a region of the sky. They are oriented symmetrically such that they have the same latitude and intersect the sky sphere forming an imaginary pyramid, whose vertex is placed at the center of the insect head. Formally, their orientation relative to the body frame B can be represented in Cartesian coordinates as follows:

$$\begin{array}{ll} P_1^b = (\sqrt{1-h^2}, 0, h), & P_2^b = (-\sqrt{1-h^2}, 0, h) \\ P_3^b = (0, \sqrt{1-h^2}, h), & P_4^b = (0, -\sqrt{1-h^2}, h) \end{array} \tag{4}$$

where the parameter $h \in (-1, 1)$ sets the latitude of the photoreceptors. Every photoreceptor collects light from a conic region A_i around its ideal orientation P_i as shown in Figure 3.1.

The most important assumption made in this part is that the intensity of light, I, measured by a photoreceptor P, is *independent* from its longitude and is a *strictly monotonically decreasing* function of its latitude only. Formally it can be written as:

$$\begin{array}{rcl} I(P) & = & I(\psi, \theta) = I(\theta) \\ \theta_1 < \theta_2 & \Rightarrow & I(\theta_1) > I(\theta_2) \end{array} \tag{5}$$

where, with an abuse of notation, we identify the position of the photoreceptor with its latitude θ, which

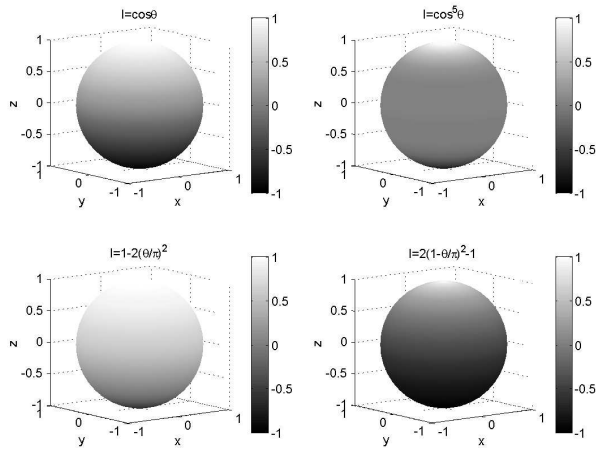

Figure 4: Light intensity distribution over the celestial sphere for different monotonic functions.

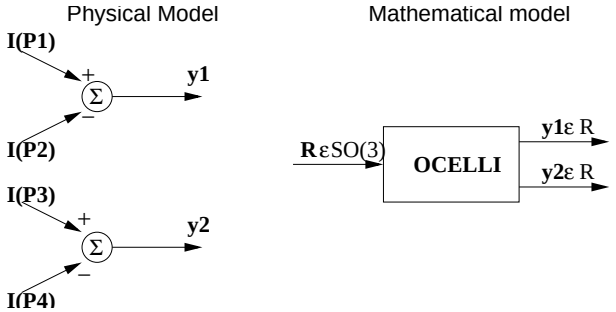

Figure 5: Physical and mathematical representation of ocelli sensory system.

is the angle between the z-axis of the fixed frame A and the orientation of the photoreceptor on the celestial sphere (see Figure 1). Figure 3.2 shows the light intensity distribution on the sky sphere for different monotonic functions of the latitude. Without loss of generality, the intensity is normalized so that $I_{max} = I(0) = 1, I_{min} = I(\pi) = -1$. The monotonic distribution of light intensity on the celestial sphere can be satisfied only in an ideal environment where the landscape is uniform and the light is diffused uniformly around its source. In reality, objects such as clouds and buildings can mine this assumption. However, we believe that this hypothesis is approximately correct for the most part of the celestial sphere around the light source.

The measurements from the photoreceptors are simply subtracted pairwise as shown in Figure 3.2 and these two signals are the output from the ocelli:

$$\begin{array}{rcl} y_1 & = & I(P_1^a) - I(P_2^a) \\ y_2 & = & I(P_3^a) - I(P_4^a) \end{array} \quad (6)$$

where P_i^a is the photoreceptor orientation in Cartesian coordinates relative to the fixed frame A. Given the orientation $R \in SO(3)$, of the insect body frame B relative to the fixed frame A, the orientation of the photoreceptor P_i relative to the fixed frame is $P_i^a = RP_i^b$. Since the orientation of the photoreceptors is fixed with respect to the body frame B, the outputs from the ocelli depend only on the insect orientation R. From a mathematical point of view, the ocelli system can be thought as a nonlinear function $f : SO(3) \to R^2$ of the insect orientation as shown in Figure 3.2.

3.3 Orientation Estimation

This section is devoted to studying the general properties of the map $f()$, *i.e.* how much information about the orientation R can be retrieved from the ocelli output. We first consider the special case where the light intensity measured by the photoreceptors is $I(\theta) = \cos\theta$. This instance clearly highlights the relation between the insect orientation R and the ocelli output y. Then, we consider general cases where $I(\theta)$ is simply monotonic.

Proposition 1 *Suppose that the light intensity measured by the photoreceptors is $I(\theta) = \cos\theta$, and let the orientation of the photoreceptors be such that $h = \frac{\sqrt{3}}{2}$ in Equations (4). Then the output of the ocelli is $y_1 = r_{31}, y_2 = r_{32}$, where r_{ij} is the $i-j$ entry of the insect orientation matrix R.*

Proof: Substituting $h = \frac{\sqrt{3}}{2}$ and $I(\theta) = \cos\theta$ into Equations (6) we get:

$$\begin{array}{rcl} y_1 & = & I(P_1^a) - I(P_2^a) = \cos\theta_{P_1^a} - \cos\theta_{P_2^a} \\ & = & e_z^T P_1^a - e_z^T P_2^a = e_z^T R P_1^b - e_z^T R P_2^b \\ & = & e_z^T R(P_1^b - P_2^b) = e_z^T R e_x = r_{31} \\ y_2 & = & \ldots = e_z^T R(P_3^b - P_4^b) = e_z^T R e_y = r_{32} \end{array} \quad (7)$$

where $e_x = [1\,0\,0]^T, e_y = [0\,1\,0]^T, e_z = [0\,0\,1]^T$. The second line follows from the fact that $\cos\theta_{P^a} = z_P = e_z^T P^a$ and that $P_i^a = RP_i^b$.$\diamond$

As described at the end of Section 2, r_{31} and r_{32} correspond to the x and y coordinates of the z-axis of the fixed frame A relative to the body insect B. In other words, the ocelli can measure the x and y position of the light source relative to the insect body. Intuitively, it is clear that this information can be used to rotate the insect body towards the light source.

When the light intensity $I(\theta)$ measured by the photoreceptors is only a *monotonically decreasing* function of the latitude, the ocelli do not estimate the exact orientation of the sun relative to the insect body frame, but they can still retrieve its approximate direction, as shown in the following proposition:

Proposition 2 *Suppose that the light intensity measured by the photoreceptors, $I(\theta)$, is unknown but a strictly monotonically decreasing function of the latitude θ. Then the output of the ocelli has the following properties:*

$$\begin{array}{ll} y_1 = 0 \Longrightarrow r_{31} = 0; & y_1 \neq 0 \Longrightarrow y_1 r_{31} > 0 \\ y_2 = 0 \Longrightarrow r_{32} = 0; & y_2 \neq 0 \Longrightarrow y_2 r_{32} > 0 \end{array} \quad (8)$$

Proof: First we recall that $\cos^{-1}()$ is a strictly monotonically decreasing function of its argument, and that the composition of two monotonically decreasing functions is a monotonically increasing function. Therefore, $\tilde{I} = I \circ \cos^{-1}()$ is a monotonically increasing function. Consider the first ocelli output y_1:

$$\begin{array}{rcl} y_1 & = & I(\theta_{P_1^a}) - I(\theta_{P_2^a}) \\ & = & I(\cos^{-1}(e_z^T P_1^a)) - I(\cos^{-1}(e_z^T P_2^a)) \\ & = & \tilde{I}(e_z^T P_1^a) - \tilde{I}(e_z^T P_2^a) \\ & = & \tilde{I}(e_z^T R P_1^b) - \tilde{I}(e_z^T R P_2^b) \\ & = & \tilde{I}(r_{31}\sqrt{1-h^2} + r_{33}h) - \ldots \\ & & \ldots - \tilde{I}(-r_{31}\sqrt{1-h^2} + r_{33}h) \end{array} \quad (9)$$

where we use the fact $\cos\theta_{P^a} = z_P = e_z^T P^a$ in the second line, and the orientations P_i^b of the photoreceptors are given by Equations (4). Let us define $l = \sqrt{1-h^2}$. Since the function $\tilde{I}$ is monotonically increasing we have:

$$\begin{aligned} y_1 > 0 \quad &\Rightarrow \quad \tilde{I}(r_{31}l + r_{33}h) > \tilde{I}(-r_{31}l + r_{33}h) \\ &\Rightarrow \quad r_{31}l + r_{33}h > -r_{31}l + r_{33}h \\ &\Rightarrow \quad 2\,r_{31}l > 0 \Rightarrow r_{31} > 0 \end{aligned} \tag{10}$$

where we use the fact that $\tilde{I}$ is monotonically increasing and that $l > 0$. Analogously, it is easy to verify that $y_1 < 0 \Rightarrow r_{31} < 0$. From monotonicity of $\tilde{I}$ also follows that $y_1 = 0 \Rightarrow r_{31} = 0$. Finally, the same arguments can be used to prove the properties of ocelli output y_2. $\diamond$

This proposition indicates that the ocelli still give an approximate position of the light source, regardless of the exact positioning of the photoreceptors relative to the insect body and regardless of the specific light intensity distribution as long as it is monotonic. Moreover, the outputs of the ocelli are zero if and only if the z-axis of the body frame is aligned with the z-axis of the fixed frame. Intuitively, if the insect rotates towards the apparent position of the light source given by the ocelli, it will eventually align the z-axes of the body and the fixed frame. This intuition is exploited when designing the stabilizing control laws for the attitude.

4 Halteres

4.1 Morphology

Research on insect flight revealed that in order to maintain stable flight, insects use structures, called halteres, to detect body rotations via gyroscopic forces [3]. The halteres of a fly evolved from hindwings and are hidden in the space between thorax and abdomen so that air current has negligible effect on them (see Figure 6). The halteres resemble small balls at the end of thin rods. There are about 400 sensilla embedded in the flexible exoskeleton at the haltere base. These mechanoreceptors function as strain gages to detect the Coriolis force exerted on the halteres [2]. During flight the halteres beat up and down in vertical planes through an angle of nearly 180^o anti-phase to the wings at the wingbeat frequency. When a fly's halteres are removed or immobilized, it quickly falls to the ground. In addition, the two halteres of a fly are non-coplanar (each is tilted backward from the transverse plane by about 30^o) so that flies can detect rotations about all three turning axes.

4.2 Modeling

A complex force, as a result of insect motion and haltere kinematics, acts on the halteres during flight [6]. Assuming no translational motion of the insect, this force can be expressed in vector notation by the following:

$$\mathbf{F} = m\mathbf{g} - m\mathbf{a} - m\dot{\boldsymbol{\omega}}\times\mathbf{r} - m\boldsymbol{\omega}\times(\boldsymbol{\omega}\times\mathbf{r}) - 2m\boldsymbol{\omega}\times\mathbf{v} \tag{11}$$

where m is the mass of the haltere, $\mathbf{r}$, $\mathbf{v}$, and $\mathbf{a}$ are the position, velocity, and acceleration of the haltere relative to the insect body, $\boldsymbol{\omega}$ and $\dot{\boldsymbol{\omega}}$ are the angular velocity and angular acceleration of the insect, and $\mathbf{g}$ is the gravitational constant. Further, this force

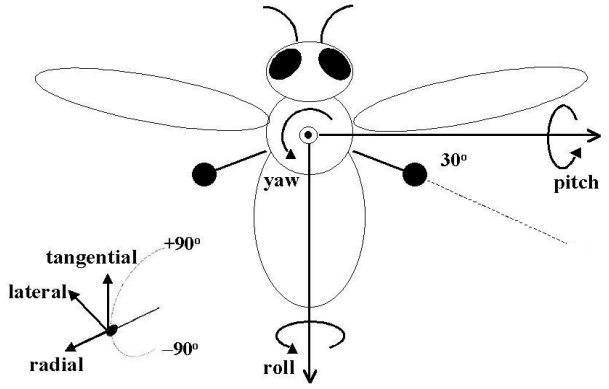

Figure 6: Schematic of enlarged halteres of a fly.

can be decomposed into radial, tangential, and lateral components as depicted by the exploded view of the haltere in Figure 6. Insect's body rotations produce centrifugal ($-m\boldsymbol{\omega}\times(\boldsymbol{\omega}\times\mathbf{r})$) and Coriolis ($-2m\boldsymbol{\omega}\times\mathbf{v}$) forces on the halteres. The centrifugal force is generally smaller than the Coriolis force and mostly in the radial and tangential directions. Moreover, the centrifugal force provides no information on the sign of rotations. The Coriolis force, on the other hand, has components in all three directions and contains information on the axis, sign, and magnitude of the insect's body rotations. The angular acceleration force ($-m\dot{\boldsymbol{\omega}}\times\mathbf{r}$) and the Coriolis force are separable because of the 90^o phase shift (they are orthogonal functions). The primary inertial force ($-m\mathbf{a}$) has only radial and tangential components and is orders of magnitude larger than the Coriolis force. The gravitational force ($m\mathbf{g}$) is always constant and depending on the haltere position and the insect's body attitude in space, its distribution in the three directions varies. However, the effect of this gravitational force on the rotation sensing is negligible because it is a tonic lateral component which can be considered as DC offset on the Coriolis force and removed by the subsequent signal processing step.

Figure 7 shows the traces of the components of the Coriolis force for rotations about the roll, pitch, and yaw axes. Note that since the Coriolis force is proportional to the cross product of the angular velocity and the instantaneous haltere velocity, there is no tangential component in the Coriolis force. In addition, to detect body rotations, the lateral forces on the halteres are measured because the large primary inertial force has no contribution in the lateral direction and hence it is possible to measure the Coriolis signal among all other interfering force signals appearing in this direction. Because of the dependence of the Coriolis force on the haltere velocity, these force signals are modulated in time with haltere beat frequency. For a roll rotation, the signal is modulated with the haltere beat frequency and the left and right signals are 180^o out-of-phase. For a pitch rotation, the signal is also modulated with the haltere beat frequency, but the left and right signals are in-phase. For a yaw rotation, the signal is modulated with double the haltere beat frequency and the left and right signals are 180^o out-of-phase.

Utilizing the characteristics (frequency, modulation, and phase) of these force signals on the left and right halteres, a demodulation scheme is proposed to decipher roll, pitch, and yaw rotations. First, a

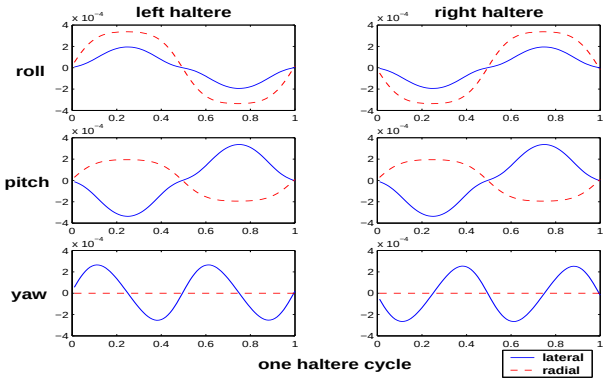

Figure 7: Coriolis force for rotations about the roll, pitch, and yaw axes.

pitch rotation can be easily distinguished from roll and yaw rotations by noting the phases of the left and right signals. Because the left and right signals are in-phase for pitch while out-of-phase for roll and yaw, adding the left and right signals retains pitch component and eliminates roll and yaw components. In order to separate roll and yaw components, the force signal is multiplied by demodulating signals of corresponding frequencies as:

$$\pm\sin(\Omega t)\cdot\sin(\Omega t) = \pm\sin^2(\Omega t) \quad (12)$$

$$\pm\sin(2\Omega t)\cdot\sin(2\Omega t) = \pm\sin^2(2\Omega t) \quad (13)$$

$$\pm\sin(\Omega t)\cdot\sin(2\Omega t) = \pm 2\sin^2(\Omega t)\cdot\cos(\Omega t) \quad (14)$$

where Ω is the haltere beat frequency.

From equations 12 and 13, it is clear that when the products are averaged over one haltere cycle, a sinusoidal signal at the haltere frequency retrieves the roll component which is modulated with the haltere beat frequency, while a sinusoidal signal at double the haltere frequency retrieves the yaw component which is modulated with double the haltere beat frequency. However, if the demodulating and force signals are at different frequencies as in equation 14, averaging the product over one haltere cycle results in zero output. Thus, this technique effectively decouples roll from yaw. Figure 8 illustrates this proposed demodulation scheme. Ideally, the magnitudes of the amplifiers, A_r, A_y, and A_p, would be proportional to $-1/2mv$, where m is the mass and v is the instantaneous velocity of the haltere.

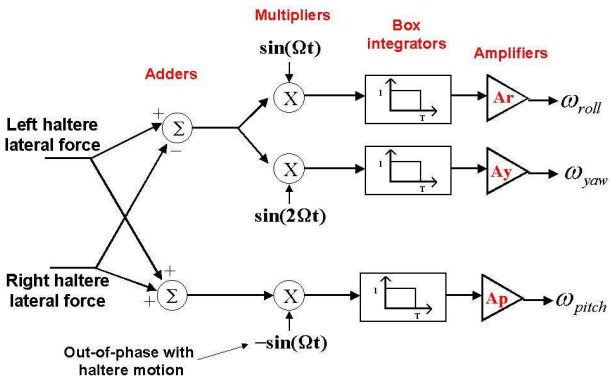

Figure 8: Demodulation scheme of haltere forces.

4.3 Simulations

The mechanism which the halteres detect angular velocities and the proposed demodulation method have been tested. In the simulations, the halteres were assumed to be phase-locked to the wings and beating in the stroke plane. These assumptions are made due to the fact that when the wings are flapping, the body of the insect would oscillate, as a result of the wing inertia, along an axis parallel to the wing stroke in the stroke plane. Since the forces orthogonal to the haltere beat plane (*i.e.* lateral forces) are sensed, it is possible to avoid the error caused by this common mode body oscillation by phase-locking the halteres to the wings in the stroke plane.

For testing the performance of the halteres, the angular velocities of an insect under hovering condition are generated by the Virtual Insect Flight Simulator (VIFS), a software testbed that is used to simulate the dynamics of the MFI and evaluate control algorithms [9]. The results are shown in Figure 9.

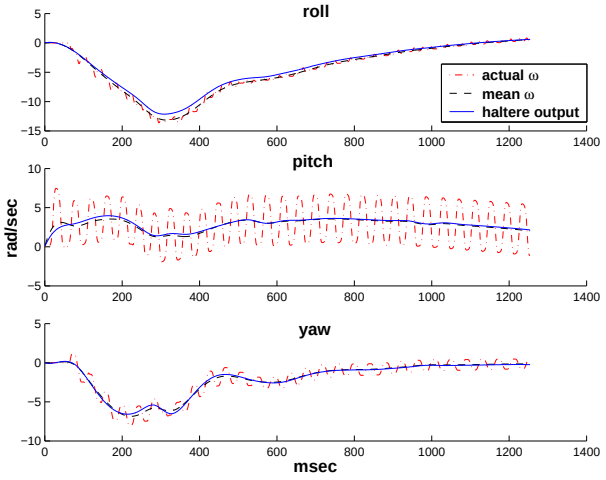

Figure 9: Angular rotation detection by halteres.

5 Attitude Stabilization via Output Feedback

In the previous sections we described how halteres can estimate the insect angular velocities relative to the body frame, and how the ocelli can estimate the position of the z-axis of the fixed frame relative to the body frame. In this section we combine the outputs from these two sensory systems to obtain a global stabilizing control law to align the z-axis of the body frame with the z-axis of the fixed frame. These two axes are aligned if and only if the angle, θ_z, between them is zero. This angle can be computed from the rotation matrix R, by recalling that *cosine* of the angle between two unit vectors is given by their inner product, *i.e.* $\cos\theta_z = e_z^T v_z^a = e_z^T R e_z = r_{33}$ where v_z represents the z-axis of the body frame. Based on the intuition that the input torque should rotate the insect body frame such that the angle θ_z would decrease, we propose the following output feedback law:

$$u = -a[y_2 \; -y_1 \; 0]^T - c\,\hat{\omega}^b \quad (15)$$

where $aandc$ are scalar and $\hat{\omega}^b$ is the haltere output.

This is shown in the following two theorems:

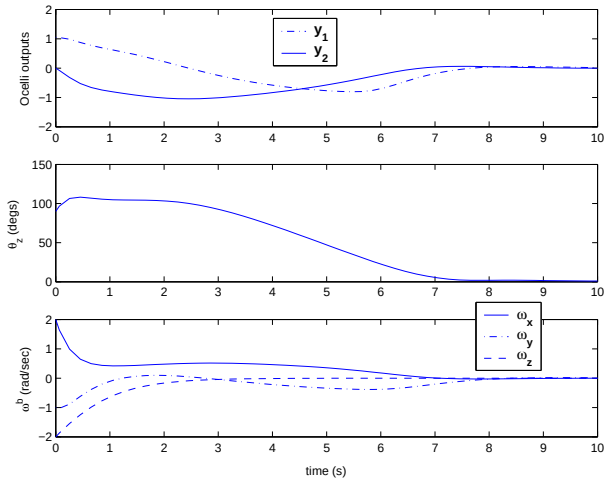

Figure 10: Simulations results of insect dynamics.

Theorem 1 *If the intensity function* $I = f(\theta) = A\cos(\theta)$*, where* $A \in R$ *is a constant, and* $a, c > 0$ *then the control law (15)* **globally** *aligns the z-axes of the fixed and body frames, i.e.* $(\theta_z = 0, \omega^b = 0)$ *is a stable equilibrium point.*

Theorem 2 *If the intensity function* $I = f(\theta)$ *is a monotonically decreasing function, then there exists a positive constant* $M > 0$ *such that the control law (15)* **globally** *aligns the z-axes of the fixed and body frames, i.e.* $(\theta_z = 0, \omega^b = 0)$ *is a stable equilibrium point, as long as* $c > Ma$*.*

In our framework "globally" means for any initial condition but $(\theta_z, \omega^b) \neq (\pi, 0)$, which corresponds to an unstable equilibrium orientation. The proofs of these two theorems are rather lengthy, and hence are omitted in this paper.

Simulations of control law (15) with light intensity function $I = \cos^5\theta$ and initial conditions $(\theta_z, \omega^b) = (\frac{\pi}{2}, -1, -2, 2)$ are shown in Figure 9. As expected, the angle between the z-axes and the insect angular velocity go to zero. This control law is very promising for three main reasons. First, it is *simple*: the input control is simply some proportional feedback of the sensors outputs. This is very important in terms of the implementation of control laws, since the MFI has very limited computational power. Second, it is *robust*: despite its simplicity, this control law does not depend on the exact light intensity function, as long as it is a monotonically decreasing function of the latitude. Third, it is *globally convergent*: remarkably, this control law guarantees the alignment of the insect vertical axis with the light source from any initial condition including the upside down orientation which are likely to occur in the presence of wind gusts.

6 Conclusions

In this work we have investigated two types of biologically inspired sensing mechanisms. The halteres have already been realized as biomimetic sensors for use on the MFI while the ocelli are under implementation. We also developed an attitude control law for the MFI using the output feedback from the halteres and ocelli. Through our work, we have shown that simple schemes (simple sensor architectures and feedback control) can achieve robust global stability. In the future, we will employ a more realistic insect body dynamics that can account for the viscous torques resulting from the body rotation, and consider limiting factors such as input torque saturation and control of the torques only on a wingbeat-by-wingbeat basis. In addition, we will address the questions on how to choose better gains a and c in the control law and how sensor noise affects the performance of the control law.

References

[1] R.S. Fearing, K.H. Chiang, M.H. Dickinson, D.L. Pick, M. Sitti, and J. Yan. Wing transmission for a micromechanical flying insect. In *Proc of the IEEE International Conference on Robotics and Automation*, pages 1509–1516, San Francisco, CA, April 2000.

[2] G. Fraenkel and J.W.S. Pringle. Halteres of flies as gyroscopic organs of equilibrium. *Nature*, 141:919–921, 1938.

[3] R. Hengstenberg. Mechanosensory control of compensatory head roll during flight in the blowfly Calliphora erythrocephala Meig. *Journal of Comparative Physiology A*, 163:151–165, 1988.

[4] B. Motazed, D. Vos, and M. Drela. Aerodymatics and flight control design for hovering MAVs. In *Proc of Amer Control Conference*, Philadelphia, PA, June 1998.

[5] R.M. Murray, Z. Li, and S.S. Sastry. *A Mathematical Introduction to Robotic Manipulation*. RCR Press, New York, 1993.

[6] G. Nalbach. The halteres of the blowfly Calliphora: I. kinematics and dynamics. *Journal of Comparative Physiology A*, 173:293–300, 1993.

[7] S. P. Sane and M. H. Dickinson. The control of flight force by a flapping wing: Lift and drag production. *Experimental Biology*, 204(204):2607–2626, June 2001.

[8] L. Schenato, X. Deng, and S. Sastry. Hovering flight for a micromechanical flying insect: Modeling and robust control synthesis. In *15th IFAC World Congress on Automatic Control*, Barcelona, Spain, July 2002.

[9] L. Schenato, X. Deng, W.C. Wu, and S. Sastry. Virtual insect flight simulator (VIFS): a software testbed for insect flight. In *Proc of the IEEE International Conference on Robotics and Automation*, pages 3885–3892, Seoul, South Korea, May 2001.

[10] H. Schuppe and R. Hengstenberg. Optica properties of the ocelli of calliphora erythrocephala and their role in the dorsal light response. *Journal of Comparative Biology A*, 173:143–149, 1993.

[11] W.C. Wu, R.J. Wood, and R.S. Fearing. Halteres for the micromechanical flying insect. In *Proc of the IEEE International Conference on Robotics and Automation*, Washington, DC, May 2002.

[12] J. Yan, R.J. Wood, S. Avadhanula, R.S. Fearing, and M. Sitti. Towards flapping wing control for a micromechanical flying insect. In *Proc of the IEEE International Conference on Robotics and Automation*, pages 3901–3908, Seoul, South Korea, May 2001.